Eur. Phys. J. A (2022) 58:102
https://doi.org/10.1140/epja/s10050-022-00751-5

THE EUROPEAN PHYSICAL JOURNAL A

Regular Article - Theoretical Physics

The role of inelastic couplings on the ^{12}C+^{12}C fusion at sub-barrier energies

L. R. Gasques[1,a], **L. C. Chamon**[1,b], **G. P. Cessel**[2,c]

[1] Universidade de Sao Paulo, Instituto de Fisica, Rua do Matao, 1371, Sao Paulo, SP 05508-090, Brazil
[2] Universidade de Sao Paulo, Instituto de Fisica, Av. Trab. Sao Carlense, 400, Sao Carlos, SP 13566-590, Brazil

Received: 29 April 2022 / Accepted: 24 May 2022 / Published online: 6 June 2022

Communicated by A. Diaz-Torres

Abstract The effect of inelastic couplings on the modified astrophysical S^*-factor for ^{12}C+^{12}C fusion reaction at sub-barrier energies is investigated using the Brazilian Nuclear Potential. The ^{12}C excited states (2^+_1, 4.44 MeV; 3^-_1, 9.64 MeV; 2^+_2, 9.84 MeV; 2^+_3, 10.3 MeV; 2^+_4, 16.1 MeV; 1^-_1, 17.2 MeV and 2^+_5, 18.8 MeV) are included in the coupling scheme. We have also coupled the 0^+_2 Hoyle state (E^* = 7.65 MeV) to the 2^+_1. In our model, the fusion cross section is associated to the absorption arising from the imaginary potential. Many resonances presented at the sub-barrier data are fairly reproduced by our approach.

1 Introduction

The fusion of two nuclei forming a compound nucleus is of paramount importance to the stellar nucleosynthesis and evolution of massive stars. In particular, the ^{12}C+^{12}C reaction, taking place at low energies ($\sim$ 1–3 MeV), has a determining role during the stellar carbon burning phase [1,2]. At such energies, the most relevant reaction branches are ^{12}C(^{12}C,p)^{23}Na (Q = 2.241 MeV) and ^{12}C(^{12}C,α)^{20}Ne (Q = 4.617 MeV). Carbon burning is also crucial for explosive scenarios like Type Ia supernovae, which are driven by carbon ignition in cores of accreting massive CO white dwarfs [3–5]. Therefore, the investigation of the ^{12}C+^{12}C reaction mechanisms has attracted a lot of attention from theoretical and experimental physicists working in the field of nuclear reactions and astrophysics.

Conventionally, fusion cross sections at very low energies, typical for astrophysical conditions, are represented by the so-called modified S^*-factor

$$S^*(E) = \sigma_F(E)\ E\ e^{(2\pi\eta + gE)}, \tag{1}$$

where $\eta = (Z_1 Z_2 e^2/\hbar)\sqrt{\mu/(2E)}$ is the Sommerfeld parameter, μ is the reduced mass, Z is the charge number of the nuclei, E is the center-of-mass energy, and g = 0.46 MeV^{-1} for ^{12}C+^{12}C. The term e^{gE} was introduced to account for the finite size of the nuclei [6].

Several phenomenological calculations have been attempted to address the ^{12}C+^{12}C fusion. Usually, such studies are based on the barrier penetration model [4,7,8] or on the ingoing-wave-boundary conditions [9,10]. Coupled-channels (CC) calculations, in which the excitations of ^{12}C are taken into account, have also been performed [11,12]. Alternatively, some recent works present the ^{12}C+^{12}C fusion results obtained with sophisticated microscopic models, such as density-constrained time dependent Hartree–Fock method [13], wave-packet dynamics within a nuclear molecular picture [14] and antisymmetrized molecular dynamics [15].

From the experimental perspective, direct fusion measurements in the laboratory are extremely challenging at very low energies. As a consequence, the ^{12}C+^{12}C fusion needs to be extrapolated to the energy region of astrophysical interest. However, due to the presence of resonant structures and discrepancies between the available data, the reliability of extrapolation models is often affected. Recently, ^{12}C+^{12}C fusion data have been measured at energies below $E_{c.m.}$ = 2.7 MeV through the indirect Trojan Horse Method (THM) [16]. The data were obtained from the ^{12}C(^{14}N,α^{20}Ne)^{2}H and ^{12}C(^{14}N,p^{23}Na)^{2}H transfer reactions. The corresponding astrophysical S^*-factor shows several resonances and a steep rise in both proton and alpha reaction branches as energy decreases. Even though, the dependability of the

L. C. Chamon, G. P. Cessel contributed equally to this work.

[a] e-mail: lgasques@if.usp.br (corresponding author)
[b] e-mail: lchamon@if.usp.br
[c] e-mail: cessel@usp.br

astrophysical S^*-factor extrapolation towards low energies is still under strong debate [17–19], and a final conclusion has not been yet achieved.

In this paper, we have focused on the description of the resonant structure present in the S^*-factor data set at sub-barrier energies through CC calculations. Here, most of the resonances have been qualitatively described by adopting a weak absorption of the imaginary part of the optical potential.

2 Theoretical framework

Recently, a new theoretical approach for the real part of the nuclear interaction between two reacting nuclei has been proposed [20]. The approach, named Brazilian Nuclear potential (BNP), is based on the double-folding method, which relies on two main ingredients: the density distributions of the nuclei and the nucleon–nucleon interaction. The ^{12}C matter density distribution can be calculated as twice the charge density, which in turn is obtained from electron scattering experiments. This procedure is fully justified since the number of protons and neutrons are the same for ^{12}C. In particular, for the ^{12}C nucleus, the proton and neutron distributions calculated with the Dirac–Hartree–Bogoliubov model are quite similar. Therefore, the hypohesis that the matter density is well described by twice the experimental charge density distribution is, in fact, a suitable assumption. Within the BNP approach, the nucleon–nucleon interaction is given by

$$v_{nn}(\vec{r}) = -U_0\, e^{-(r/a)^2}, \tag{2}$$

with $U_0 = 87.226$ MeV and $a = 0.95$ fm.

In this paper, the BNP has been used within the context of the CC formalism to calculate the sub-barrier ^{12}C+^{12}C fusion cross sections (the s-wave barrier height is $V_B \sim 6.2$ MeV). We have also calculated the Coulomb potential through the double-folding procedure [20]. An imaginary optical potential, $W(r)$, is adopted to simulate the corresponding absorption by the fusion process. The fusion probability for each J value is obtained from

$$P_J(E) = -\frac{4k}{E}\sum_{\alpha}\int_0^{\infty} W(r)\,|\chi^{(+)}_{\alpha,J}(r)|^2\,dr, \tag{3}$$

where $\chi^{(+)}_{\alpha,J}$ represent the radial wave functions and α accounts for all the coupled equations included in the calculations [21,22]. The total fusion cross section is obtained as

$$\sigma_F(E) = \frac{2\pi}{k^2}\sum_{J\ even}(2J+1)P_J(E), \tag{4}$$

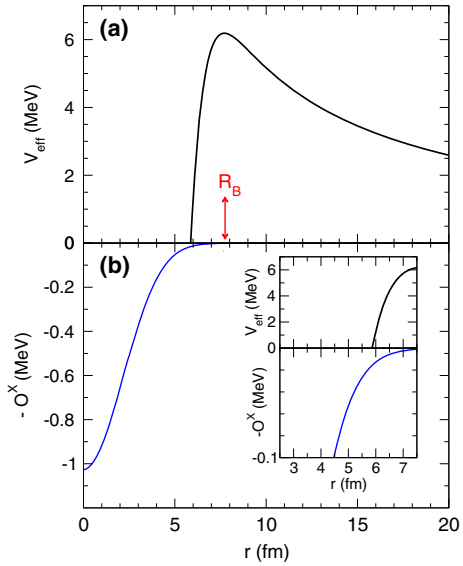

Fig. 1 **a** Effective potential for $\ell = 0$. **b** Imaginary potential given by Eq. (5) assuming $N_i = 1$ MeV fm^3. The arrow in the figure indicates the position of the barrier radius (R_B). The inset shows a magnification of the imaginary potential in the Coulomb barrier region

being k the wave number. As the interaction is between two identical nuclei with 0^+_1 ground-state, J can only take even values.

In our approach, the imaginary potential is defined as

$$W_J(r) = -N_i \times O(r), \tag{5}$$

$$O(r) = \int \rho_m(r_1)\,\rho_m(r_2)\,\delta(\vec{r}-\vec{r}_1+\vec{r}_2)\,d\vec{r}_1\,d\vec{r}_2, \tag{6}$$

where ρ_m is the ground-state ^{12}C matter distribution. Due to the delta function in the integral of Eq. (6), the term $O(r)$ represents the convolution of both densities as a function of the internuclear distance. In this approach, the fusion probability is related to the overlap of the densities, being the parameter N_i of Eq. (5) employed to adjust this correlation. We consider this approach for the imaginary potential more realistic than the Woods–Saxon form usually assumed in many works, since its shape is directly related to the convolution of the nuclear densities. In this approach, the short range imaginary potential must account for the fusion process.

For illustration, the ^{12}C+^{12}C effective potential $V_{eff} = V_N(r) + V_C(r)$ for $\ell = 0$ is plotted in panel (a) of Fig. 1, where $V_N(r)$ and $V_C(r)$ refer to the nuclear (BNP) and the Coulomb potentials, respectively. The arrow in the figure indicates the position of the barrier radius (R_B). The imaginary potential given by Eq. 5 is shown in panel (b). The curve was obtained assuming $N_i = 1$ MeV fm^3. As can be noted in the inset, the imaginary potential extends to the region near the barrier radius.

Table 1 Spin, excitation energies (MeV), transition amplitudes (10^{-3} e^2b^λ) and deformation lengths (fm) for the ^{12}C excited states included in the CC calculations

J_i	E^*	J_f	E^*	λ	$B(E\lambda)\uparrow$	δ_λ
0_1^+	0.00	2_1^+	4.44	2	3.966	1.42
0_1^+	0.00	3_1^-	9.64	3	0.251	1.66
0_1^+	0.00	2_2^+	9.84	2	0.160	0.29
0_1^+	0.00	2_3^+	10.3	2	0.367	0.43
0_1^+	0.00	2_4^+	16.1	2	0.326	0.41
0_1^+	0.00	1_1^-	17.2	1	2.433	0.24
0_1^+	0.00	2_5^+	18.8	2	0.106	0.23
2_1^+	4.44	0_2^+	7.65	2	0.269	0.37

The CC calculations were performed using the FRESCO code [23]. As already mentioned, the cross sections were obtained considering only even angular momentum values. In the CC scheme, we included all ^{12}C excited states coupled directly to the ground-state, for which the electric transition values are published in the literature: (2_1^+, 4.44 MeV; 3_1^-, 9.64 MeV; 2_2^+, 9.84 MeV; 2_3^+, 10.3 MeV; 2_4^+, 16.1 MeV; 1_1^-, 17.2 MeV and 2_5^+, 18.8 MeV). In addition, we have also coupled the 0^+ Hoyle state (E^* = 7.65 MeV) to the first 2_1^+ excited state. In spite of being a second order transition, the effect of considering the Hoyle state in the coupling scheme is not negligible. The corresponding transition probabilities were taken from the NNDC database [24]. The nuclear deformation δ_λ values were calculated from the respective Coulomb transition probabilities, considering the effect of the finite diffuseness value of the nuclear density [25]. Details of the coupling parameters are given in Table 1.

3 Results

Generally, previous theoretical results for S^*-factors published in the literature show good agreement with the data (see, e.g., [18]). However, in most of these works only an average description of the data (neglecting resonant oscillations) is reproduced satisfactorily. Here, our main interest concerns the description of the pronounced resonant structures of the sub-barrier ^{12}C+^{12}C S^*-factor. In our approach, the fusion cross section is associated to the absorption arising from the imaginary potential. Therefore, the choice of a weak absorptive imaginary interaction could reveal underlying structures related to the real part of the optical potential (virtual states of the potential). Similar behavior was already reported, for instance, in the case of α +^{12}C [22]. In addition, two-center shell model calculations revealed the importance of the nonaxial symmetric configurations for the formation of molecular resonances for the ^{12}C+^{12}C reaction [26]. As a consequence, most ^{12}C+^{12}C di-nuclear configurations experience a rather weak absorption, leading to potential resonances [14].

In order to reproduce, as well as possible, the magnitude and the resonant behavior of the S^*-factor data, two adjustable parameters have been assumed in our CC calculations: N_r and N_i. At the present paper, we have adopted an J-dependent optical potential. Indeed, the polarization potential that arises from couplings is energy and angular momentum dependent, and therefore the optical potential should also present such a characteristic [27]. The assumption that the optical potential does not depend on the angular momentum is just a simplification that works well for many systems at energies above the barrier.

Variations in the N_r and N_i parameter values modify the width and the magnitude of the calculated fusion cross sections. The corresponding position of the centroid of each resonance can be fine-tuned by small modifications of the real part of the nuclear interaction. Thus, for each J value, the BNP has been multiplied by a normalization factor N_r. The N_i parameter value, assumed as J independent, was varied to fit the data. According to our calculations, only the first partial waves ($0 \leq J \leq 4$) contribute significantly to the fusion cross sections at the energies tackled in the present work. The N_r values resulting from the CC analyses are 1.0368, 0.9300 and 1.0695, for J = 0, 2 and 4, respectively. As can be noticed, the values of N_r are close to unity, indicating that the BNP is realistic. For the determination of the imaginary potential, we have obtained N_i = 1 MeV fm^3. In such conditions, the strength of the imaginary part of the optical potential is about 400 times lower than that of the real part, corroborating the weak absorption regime.

Figure 2 presents the experimentally determined S^*-factor data at energies below the Coulomb barrier [16,28–32]. The dotted green and solid black lines in the figure were obtained from optical model single-channel (SC) and CC calculations, respectively. As can be observed, concerning the SC calculations, a strong resonance appears around the 3 MeV energy region, while fixing the N_r values for J = 0, 2 and 4, as 1.0368, 0.9300 and 1.0695, respectively. This behavior is due to the choice of the N_r parameter values upon the condition of a weak absorptive imaginary potential. On the other hand, this resonance disappears and the centroid and the width of some other resonances present in the data are fairly described by CC calculations, demonstrating that the effect of the inelastic couplings on the fusion cross sections is quite significant. Indeed, a direct comparison of the curves shown in Fig. 2 reveals that several resonances are related to the inelastic couplings. We point out that our calculations describe the average behavior of the THM data [16]. However, as we have already commented, there is some debate regarding the prescription employed to extract the corresponding cross sections. It is important to mention that, the increasing trend of the calculated S^*-factor curve at extreme sub-barrier ener-

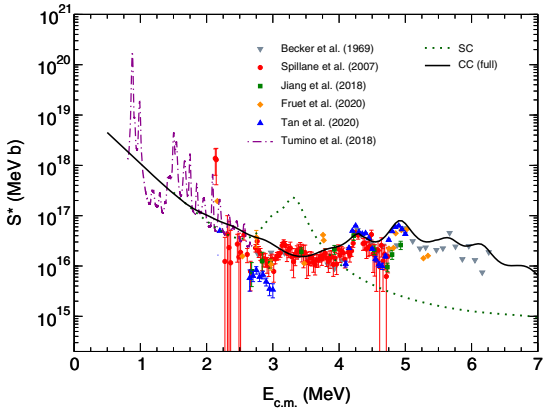

Fig. 2 Modified S^*-factor as a function of the center-of-mass energy for ^{12}C+^{12}C. The data are taken from Refs. [16,28–32]. The solid black was calculated within the CC framework, while the dotted green curve was obtained without considering the coupling (SC) to inelastic states of ^{12}C

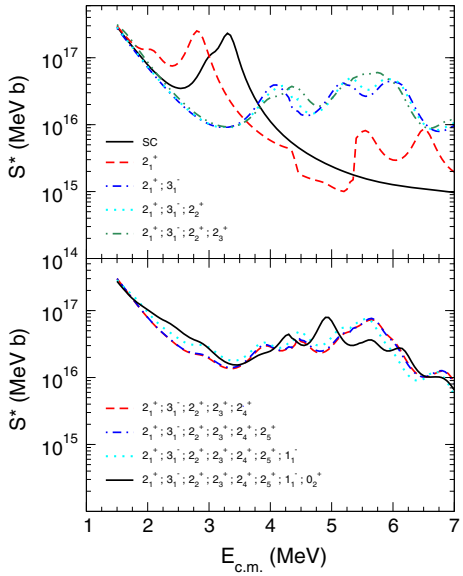

Fig. 3 CC calculations for the ^{12}C+^{12}C reaction. Each curve was obtained considering different sets of excited states in the coupling scheme

gies is related to the geometry of the imaginary potential, which extends outside the inner region of the Coulomb barrier (see Fig. 1). Because of this, the absorption of flux starts from relatively larger distances, enhancing significantly the calculated sub-barrier S^*-factors. Since the imaginary potential can not be obtained from fundamental grounds, there is a degree of uncertainty regarding the behavior of the ^{12}C+^{12}C fusion towards extreme low energies, from both experimental and theoretical analyses. In fact, some models predict a decrease of the S^*-factor as $E_{c.m.}$ becomes smaller [33,34].

Figure 3 shows CC calculations for the ^{12}C+^{12}C reaction. Each curve was obtained considering different sets of excited states in the coupling scheme. The N_r values of 1.0368, 0.9300 and 1.0695 were kept constant for $J = 0$, 2 and 4, respectively. The effect of including individual channels can be directly observed in both panels of the figure. Clearly, some states have a greater impact than others in the calculated S^*-factor, but altogether are important for the description of the experimental cross section data. As we have already mentioned, we included only those ^{12}C excited states in which the electric transition values are found in the literature. Depending on these values, the inclusion of some other excited states, such as the 13.30 MeV 4_1^+ and 14.08 MeV 4_2^+, might have a significant impact on the fusion cross sections calculated within the CC formalism.

4 Discussion and summary

In summary, we investigated the ^{12}C+^{12}C fusion cross sections at sub-barrier energies using the BNP interaction. In our model, the imaginary potential simulates the absorption of flux from the elastic and inelastic channels to the fusion process. By assuming weak absorption of the imaginary part of the optical potential at low energies, several resonances observed in the fusion data have been qualitatively described by our model. Such resonances can be associated to virtual molecular states involving the two carbons, that would present significant superposition with states of the ^{24}Mg compound nucleus resulting in nuclear fusion. In order to fine-tune the position of the centroid of the resonances, the BNP interaction has been renormalized for each partial wave by factors quite close to unity. Of course, we do not describe all the resonances presented in the fusion data sets, since some of them are not related to the ^{12}C+^{12}C configurations of ^{24}Mg.

We have unambiguously demonstrated that the couplings to inelastic states play a crucial role in the description of the fusion cross sections. Besides the first 2_1^+ ^{12}C excited state at 4.44 MeV, usually considered in the CC calculations performed in previous works, we have included several other states in our approach. Clearly, the effect of these other couplings is of relevance for describing the behavior of the S^*-factor data.

Considering the importance of the ^{12}C+^{12}C reaction in different astrophysical scenarios, it would be desirable to investigate the effects of increasing the number of channels included in the CC calculations. Therefore, the experimental determination of the transition amplitudes related to other ^{12}C excited states could improve the description of the sub-barrier fusion data. For instance, depending on the deformation parameter values related to the transition of the 13.30 MeV 4_1^+ and 14.08 MeV 4_2^+ states to the 4.44 MeV 2_1^+ state, the calculated S^*-factors could be significantly modified.

Acknowledgements L. R. Gasques is grateful to A. Diaz-Torres and J. Lubian for the valuable discussions. This work was partially supported by Fundação de Amparo à Pesquisa do Estado de São Paulo (FAPESP) Proc. No 2019/07767-1 and 2021/04332-4, Conselho Nacional de Desenvolvimento Científico e Tecnológico (CNPq) Proc. No 406332/2018-5, 302160/2018-3, 304056/2019-7, and project INCT-FNA Proc. No 464898/2014-5.

Data Availability Statement This manuscript has no associated data or the data will not be deposited. [Authors' comment: This is a theoretical paper therefore the data presented a here have been published earlier by their corresponding authors.]

References

1. C.A. Barnes, S. Trentalange, S.C. Wu, Treatise on Heavy-Ion Science, vol. 6 (Plenum, New York, 1985), p. 3, Nuclear Astrophysics (**edited by D. A. Bromley**)
2. M.E. Bennett et al., Mon. Not. R. Astron. Soc. **420**, 3047 (2012)
3. W. Hillebrandt, J.C. Niemeyer, Annu. Rev. Astron. Astrophys. **38**, 191 (2000)
4. L.R. Gasques, A.V. Afanasjev, E.F. Aguilera, M. Beard, L.C. Chamon, P. Ring, M. Wiescher, D.G. Yakovlev, Phys. Rev. C **72**, 025806 (2005)
5. A. Parikh, J. José, I.R. Seitenzahl, F.K. Röpke, Astron. Astrophys. **557**, A3 (2013)
6. J.R. Patterson, H. Winkler, C.S. Zaidins, Astrophys. J **157**, 367 (1969)
7. V.Y. Denisov, N.A. Pilipenko et al., Phys. Rev. C **81**, 025805 (2010)
8. E.F. Aguilera et al., Phys. Rev. C **73**, 064601 (2006)
9. P. Christensen, Z. Switkowski et al., Nucl. Phys. A **280**, 205 (1977)
10. H. Esbensen, X. Tang, C.L. Jiang et al., Phys. Rev. C **84**, 064613 (2011)
11. C.L. Jiang, B.B. Back, H. Esbensen, R.V.F. Janssens, K.E. Rehm, R.J. Charity et al., Phys. Rev. Lett. **110**, 072701 (2013)
12. M. Assunção, P. Descouvemount et al., Phys. Lett. B **723**, 355 (2013)
13. A.S. Umar, V.E. Oberacker, C.J. Horowitz et al., Phys. Rev. C **85**, 055801 (2012)
14. A. Diaz-Torres, M. Wiescher, Phys. Rev. C **97**, 055802 (2018)
15. Y. Taniguchi, M. Kimura, Phys. Lett. B **823**, 136790 (2021)
16. A. Tumino et al., Nature **557**, 687 (2018)
17. A.M. Mukhamedzhanov, D.Y. Pang, A.S. Kadyrov et al., Phys. Rev. C **99**, 064618 (2019)
18. C. Beck, A.M. Mukhamedzhanov, X. Tang, Eur. Phys. J. A **56**, 87 (2020)
19. A.M. Mukhamedzhanov et al., Eur. Phys. J. A **58**, 71 (2022)
20. L.C. Chamon, B.V. Carlson, L.R. Gasques, Comput. Phys. Commun. **267**, 108061 (2021)
21. G.R. Satchler, M.A. Nagarajan, J.S. Lilley, I.J. Thompson, Ann. Phys. **178**, 110 (1987)
22. L.C. Chamon, L.R. Gasques, L.F.M. Alves, V. Guimarães, P. Descouvemount, R.J. de Boer, M. Wiescher, J. Phys. G **41**, 035101 (2014)
23. I.J. Thompson, Comp. Phys. Rep. **7**, 167 (1988)
24. Evaluated Nuclear Structure Data File. https://www.nndc.bnl.gov/nudat2/
25. L.C. Chamon, B.V. Carlson, Nucl. Phys. A **846**, 1 (2010)
26. A. Diaz-Torres, Phys. Rev. Lett. **101**, 122501 (2008)
27. G.R. Satchler, *Direct Nuclear Reaction* (Clarendon, Oxford University Press, 1983)
28. H.W. Becker et al., Z. Phys. A **303**, 305 (1981)
29. T. Spillane et al., Phys. Rev. Lett. **98**, 122501 (2007)
30. C.L. Jiang et al., Phys. Rev. C **97**, 012801(R) (2018)
31. W.P. Tan et al., Phys. Rev. Lett. **124**, 192702 (2020)
32. G. Fruet et al., Phys. Rev. Lett. **124**, 192701 (2020)
33. L.R. Gasques, E.F. Brown, A. Chieffi, C.L. Jiang, M. Limongi, C. Rolfs, M. Wiescher, D.G. Yakovlev, Phys. Rev. C **76**, 035802 (2007)
34. V.V. Sargsyan, G.G. Adamian, N.V. Antonenko, H. Lenske, Phys. Lett. B **824**, 136792 (2022)